Macromolecular Research

Article

DOI 10.1007/s13233-022-0061-5

www.springer.com/13233 pISSN 1598-5032 eISSN 2092-7673

Bi-Functional Aspects of Peptide Decorated PLGA Nanocarriers for Enhanced Translocation Across the Blood-Brain Barrier through Macropinocytosis

Ane Nishitha Vijayan[1,2]
Janani Indrakumar[3]
Sankaranarayanan Gomathinayagam[3]
Kodiveri Muthukaliannan Gothandam[3]
Purna Sai Korrapati*[,1,2]

[1] Biological Materials Laboratory, CSIR-Central Leather Research Institute (CSIR-CLRI), Adyar, Chennai, Tamil Nadu, 600020, India
[2] Academy of Scientific and Innovative Research (AcSIR), Ghaziabad 201002, India
[3] School of Biosciences and Technology, Vellore Institute of Technology, Vellore, India

Received January 12, 2022 / Revised March 23, 2022 / Accepted March 31, 2022

Abstract: The blood-brain barrier (BBB) curtails the permeability of neuroprotective drugs to the brain thus restricting the effective delivery of therapeutics for neurodegenerative disorders. Recently, greater emphasis has been given for polymeric nanoparticles as a potential delivery system to transport drugs across the blood-brain barrier. This study focuses on the cellular route, localization and enhancement of uptake of drug loaded polymeric nanoparticles for delivery across the blood-brain barrier. We have optimized and synthesized polylactic-*co*-glycolic acid (PLGA) nanoparticles as a carrier for the delivery of drugs across the barrier. Cell penetrating peptide trans-activating transcriptor (TAT) was conjugated with the polymer through covalent bonding for increasing the efficiency of drug delivery across the BBB. Rhodamine-B was used as a model drug to study the release of drugs from the synthesized nanoparticle and finally the *in vivo* uptake in a mice model was checked. The size of the synthesized nanoparticles was in the nanometer range and the release profile revealed a rapid release appropriate for brain delivery. The cellular uptake experiments revealed that the peptide conjugated nanoparticle was readily taken up by the cells through macropinocytosis. Finally, to overcome the challenges for drugs to cross the BBB in an *in vivo* system, we have tracked the bioavailability of the nanoparticles in a mice model. Here we report an enhanced uptake of the peptide functionalized drug delivery carrier to successfully deliver and track therapeutic molecules across the blood-brain barrier *in vivo*.

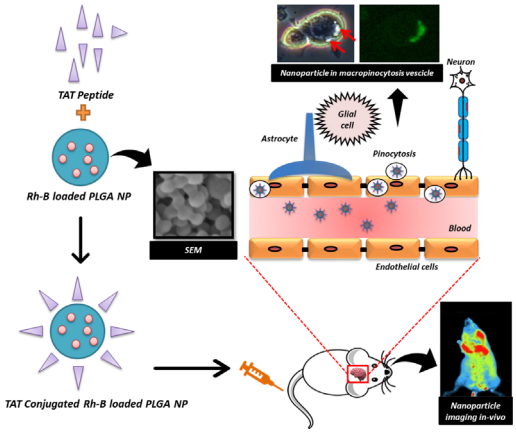

Keywords: TAT-mediated nanoparticle delivery, BBB, neurodegeneration, endocytosis, *in vivo* imaging.

Introduction

Neurodegenerative diseases affect the brain and the spinal cord, thereby having greater impact on the socio-economic status of the affected individuals. Disorders like Alzheimer's, Parkinson's *etc*. affect the neurons resulting in ataxias (motor dysfunction) or dementias (mental dysfunctioning). Effective drug delivery to the brain encompasses numerous challenges due to the multi-level barriers possessed by our nervous system. The blood-brain barrier (BBB) being the foremost hurdle for the therapeutics to encounter, is composed of endothelial cells with tight junctions. These specialized endothelial cells limit the permeability of the molecules entering the brain through various proteins like claudins, occludins and adhesion proteins.[1-3] Besides, the efflux carriers like P-glycoprotein (P-gp) toss any foreign moiety entering the BBB.[4] Hence, for the transport of therapeutic molecules to the brain, invasive and non-invasive methods are used. While invasive methods change the permeability of the blood-brain barrier, non-invasive methods offer greater advantages without disrupting the barrier.

Non-invasive techniques depend greatly on the nanotechnological advances in the recent years. Nanoparticles, nanofibers, nanotubes have emerged as a potential therapeutics in the field of medicine, owing to its wide applications and adaptations. Amongst them, polymeric nanoparticles have gained attention as drug delivery carriers due to their compatibility with biological models, sustained drug release, targeted delivery *etc*. Nanoparticles synthesized in the range of 10-1,000 nm can efficiently transport drugs across the BBB due to their smaller size. Moreover, surface modifications like PEGylation on these nanoparticles render them biocompatible and hence can be used as an efficient delivery carrier in biological systems.[5-7] Therefore, we

The original online version of this article was revised.

Acknowledgment: This research is carried out as a part of Ph.D. work registered at the Academy of Scientific and Innovative Research (AcSIR). The first author acknowledges, DST, Government of India for the financial support in the form of DST INSPIRE SRF (IF160491). The author would also like to thank CSIR FBR project SCOPE (MLP2003) for providing financial aid. The authors also express their gratitude to CSIR- Central Leather Research Institute CATERS for carrying out the physicochemical characterization. Further, the authors are grateful to the Director, CSIR-CLRI for his support and providing the required infrastructure to carry out the research (Institutional Communication number: 1547).

***Corresponding Author:** Purna Sai Korrapati (purnasai@clri.res.in)

aimed to synthesize an image-guided nanotized delivery carrier that can efficiently translocate across the BBB.

To this end, we have used the polymer PLGA as a delivery carrier to cross the BBB. PLGA (polylactic-co-glycolic acid) is an FDA approved copolymer with excellent biocompatibility and biodegradability. Many metabolic pathways produce glycolic acid and lactic acid as the byproducts and therefore degradation products of PLGA are eliminated without toxicity and immunogenicity issues, particularly for delivery to the brain.[1,8,9] Rhodamine B (Rh-B) was used as a sample drug to analyze and understand the loading and release behavior and also as a potential fluorescent marker for tracking the cells *in vitro*.[10-12] Cellular uptake by the endothelial cells lining the barrier is an immense challenge and the course of uptake also plays a major role in drug design and delivery. Therefore, to increase the nanoparticle delivery efficiency through the BBB, cell penetrating peptides (cpp) are being conjugated to the nanoparticles. Trans-activating transcriptor (TAT) peptide, a cationic peptide derived from the HIV-1 virus is used for delivering cargos to the brain because of their ability to transfer molecules without disrupting the BBB. It has been previously proven that TAT peptides can even translocate large molecules like β galactosidase and supramolecular nanostructures in the tissue culture.[13-15] Receptor mediated transport using lactoferrin, transferrin receptors require the right ligands for effective transport. Nevertheless, receptor saturation and expression of these receptors in different tissues and cells pose a disadvantage. In this regard, cationic peptides provide additional advantage without the need for receptor targeting for the transport of larger molecules through endocytic vesicles.[13,16,17] Hence, TAT peptide was chosen for the transport of the nano-carrier across the BBB.

Nanoparticle based delivery in an *in vivo* system depends on the nano-cell interactions, microenvironment, route of administration *etc*.[18] While there are numerous reports that emphasis on the delivery of drugs across the BBB, very few carriers have entered clinical trials because of the complexity of the biological models with respect to the uptake of the nanoparticulate system.[2,19-21]

Hence, the particle size, delivery route, uptake mechanism are vital for successful delivery of drugs to the BBB. In this report, we have standardized the synthesis technique and parameters to produce image-guided polymeric nanocarriers with optimal size and stability which is essential for drug delivery to the brain. Moreover, the synthesized nanoparticles were surface modified with TAT peptide for enhanced uptake and the endocytic route of uptake was studied. We have also shown that the synthesized TAT peptide conjugated RhB-PLGA carriers are efficient in crossing the BBB in an *in vivo* system in real time.

2. Experimental

2.1. Materials

Polylactic-co-glycolic acid (PLGA) 75:25 (Mw: 66,000-107,000), poly-vinyl alcohol (PVA) (Mw: 85,000-124,000), nystatin, chlorpromazine and colchicine were purchased from Sigma Aldrich. Dichloromethane and methanol were purchased from SD fine chem. Ltd, Mumbai, India. TAT peptide and TAT peptide conjugated with FITC were synthesized by Sigma Aldrich. AHNAK antibody was purchased from Santa Cruz. Water used in the experiments was purified through Millipore systems (Millipore, USA). All other chemicals and solvents used were of analytical grade.

2.2. Nanoparticle synthesis

PLGA nanoparticles were synthesized using solvent emulsion and nano-precipitation methods. For the emulsion method, PLGA was dissolved in dichloromethane (DCM) at 2.5% w/v. Dissolved PLGA solution was then added dropwise into 5% w/v PVA at 1:2 ratio under constant vortexing and probe sonicated with 10s burst at 40% amplitude. The resulting emulsion was then added to 50 mL of 0.3% PVA w/v and stirred for 3 h for complete evaporation of the solvent. Nanoparticles synthesized were recovered through centrifugation at 20,000g for 20 min and washed thrice with deionized water. Nanoparticles were resuspended in water, lyophilized (SCANVAC Coolsafe, Denmark) and stored at -20 ℃.

For nano-precipitation, 60 mg of PLGA copolymer (0.25% w/v) was dissolved in DCM:acetone:methanol mix. The ratio of the solvent combination was standardized by changing the concentration of Acetone and optimized at the ratio of 0.5:20:5 (DCM:acetone:methanol). This solution was then added drop wise to 0.05% PVA under continuous stirring for 3-4 h at 6,000 rpm to evaporate the organic solvent. The solvent to anti-solvent ratio was fixed at 1:2. For the dye loaded nanoparticles, 10 µL of the dye (rhodamine stock 0.1 µM) was dissolved in the organic phase. This mixture was then added dropwise to 0.05% PVA at the same ratio. Unloaded dye was washed off by centrifugation in double distilled (milliQ) water. The resulting nanoparticles were lyophilized and stored at -20 ℃ (SCANVAC Coolsafe, Denmark). Since nano-precipitation yielded nanoparticles of smaller size it was standardized and used further.

2.3. Peptide functionalization of the nanoparticles

For enabling uptake across the BBB, PLGA nanoparticles (PNP) were tagged with the TAT peptide. TAT peptide was conjugated to the nanoparticles with the carbodiimide (EDC/NHS) chemistry. PLGA NPs (10 mg) were activated in 0.1 M MES buffer and incubated with 100 µL of EDC/NHS in the same ratio at 4 ℃ for 1 h. To the activated nanoparticles, 500 µL of TAT was added (1 mg/mL in phosphate buffered saline (PBS)) and incubated at RT for 3 h.[22] After the incubation period, the nanoparticles were collected by ultracentrifugation and the unconjugated peptides were washed off in milliQ water.

2.4. Physico-chemical properties of the nanoparticles

Dynamic light scattering method was used to analyze the particle size of the synthesized nanoparticles. Nanoparticles were dispersed in water and 1 mL of the solution was used for the analysis. Surface morphology and size of the nanoparticles were further confirmed by using field emission scanning electron microscopy (TESCAN, Clara). 100-200 µL of the nanoparticle solu-

tion was dried in a cover slip and used for the analysis. The elemental composition of the nanoparticles encapsulated with dye was assessed by Fourier-transformed infrared spectroscopy (Perkin-Elmer, USA). The nanoparticles (PLGA, PLGA with rhodamine (Rh-B PNP) and TAT conjugated PLGA nanoparticles (Rh-B Cp PNP)) were mixed with Potassium bromide (KBr) and pressed into pellets. These pellets were used for FT-IR analysis. The elemental composition before and after peptide conjugation was examined using an XPS system. The spectra were recorded for C1s, N1s, O1s and the binding energies (eV) were calculated. Yield of the lyophilized nanoparticles after synthesis was calculated by the formula:

$$\% \text{ Yield} = \frac{\text{Weight of nanoparticles obtained}}{\text{Weight of nanoparticle used for synthesis}} \times 100 \quad (1)$$

2.5. TNBS assay

Trinitro benzene sulfonic acid (TNBS) assay was used to quantitate the primary amine groups present in the nanoparticles. Briefly, 4 mg of nanoparticle (Peptide conjugated) and equal volume of TAT peptide used for conjugation were measured and incubated with 4% $NaHCO_3$ at room temperature. After 30 minutes, 1 mL of 0.5% TNBS was added and incubated at 40 ℃ for 2 h. To this mixture, 6N HCL was added and incubated for 1 h at 60 ℃. Absorbance was measured at 335 nm (Bio-Rad, USA).

2.6. Release of rhodamine from the nanoparticles

The *in vitro* release of the fluorescent dye Rhodamine B (Rh-B) was determined by fluorescent spectroscopy. Nanoparticles (1 mg/mL) were suspended in PBS (pH 7.4, 37 ± 2 ℃) and incubated at 37 ℃ with orbital shaking. At predetermined time intervals, 1 mL of the solution was removed followed by replacement of equal volume PBS. The fluorescence was measured at an emission wavelength 574 nm using TECAN Bio instrument. The results were plotted against time and percentage. All the experiments were replicated in triplicates and the results were reported as average values. Similarly, the loading of Rh-B in PLGA NPs was obtained after dissolving the nanoparticles in the solution and then measuring the fluorescence at 574 nm (Infinite 200 pro, TECAN systems).

2.7. Biostability analysis of the synthesized nanoparticles

Stability of the synthesized nanoparticle (Rh-B PNP) in biological medium (PBS-pH 7.4, DMEM, DMEM with 10% FBS) was analyzed by measuring the particle size as a function of time. Briefly, 10 mg nanoparticles were dispersed in 10 mL of PBS, DMEM or DMEM with FBS and at regular intervals, 1 mL solution was used for the analysis.

2.8. Cell culture

Neuroblastoma (N2A) cells were used for the study. Cells were cultured in DMEM high glucose with 10% FBS and supplemented with Ampicillin (1 mg/mL), 1% penicillin/streptomycin/gentamycin under a humidified environment at 37 ℃ and 5% CO_2 (Binder, Germany).

2.9. Cell viability assay

Cytotoxicity of the PLGA nanoparticles and rhodamine-labelled nanoparticles were determined by MTT (3-(4,5-dimethylthiazol-2-yl)-2,5-diphenyltetrazolium bromide) assay in N2A cells. Cells were seeded at a density of 2×10^4 in a 48 well plate. Nanoparticles were added in different concentration in triplicates once the cells reached confluence (10-100 μg/mL). After incubating for about 24 h, cells were washed thrice with PBS and 100 μL of MTT was added to each well. Cells were incubated at 37 ℃ for 3-4 h and then 50 μL of DMSO was added to the purple formazan crystals. Readings were taken at 570/630 nm using the plate reader (Bio-Rad, USA).

2.10. AO/PI staining

The cytotoxicity of the cpp-tagged nanoparticles (Cp-PNP) was determined through acridine orange (AO) and propidium iodide (PI) staining. Cells were seeded at a density of 2×10^4 cells/well and once the cells reached confluence, NPs (PNP and Cp-PNP) were added at different concentrations. After 24 h of treatment, cells were washed and stained with AO (2 μg/mL) for 10 min at 37 ℃. PI was then added at a final concentration of 4 μg/mL (1 mg/mL stock) and incubated for 5 min. Cells were then washed and visualized under Leica microscope (Leica microsysytem, Germany).

2.11. Hemolysis assay

The effect of the nanoparticles on blood compatibility was determined by the Hemolysis assay as previously described (Sai *et al.*, 2001). Freshly collected blood was washed thrice with HEPES buffer and aliquots of 1 mL suspension containing 10^8 cells were incubated with 1 mg of the nanoparticle for half an hour at 37 ℃. Water served as a positive control (100% lysis) and the buffer served as a negative control. The suspensions were then centrifuged and 200 μL supernatant was added to a plate reader (Bio-Rad, USA). Absorbance was measured at 540 nm and % hemolysis was calculated using the formula:

$$\% \text{ Hemolysis} = \frac{\text{Absorbance of sample} - \text{Absorbance of negative control}}{\text{Absorbance of positive control} - \text{Absorbance of negative control}} \times 100 \quad (2)$$

2.12. Cellular uptake of nanoparticles

Uptake of nanoparticles by the cells was carried out using fluorescent microscopy and FACS analysis. Both the conjugated and unconjugated PLGA nanoparticles were used to determine cellular uptake efficiency. Neuro2A (N2A) cells were seeded at a density of 2×10^4 per well in a 24 well plate for the fluores-

cent analysis. Nanoparticles were added in previously determined concentration (50 μg/mL) after reaching confluence and were allowed to grow. After 24 h of incubation, cells were visualized under the Leica fluorescence microscope (Leica microsystem, Germany).

For FACS analysis, cells were seeded in a 6 well plate at a density of 5×10^5 per well and incubated at 37 ℃ and 5% CO_2. After preincubation with the nanoparticles (50 μg/mL in complete medium) for 24 h, cells were washed with ice cold PBS and collected after trypsinization (BD FACS Verse, USA).

2.13. Uptake inhibition experiment

Uptake inhibition assay was determined using different endocytic inhibitors and the percentage of uptake was measured using microscopy and flow cytometry. Nystatin, Chlorpromazine and Colchicine were used to inhibit caveolae mediated endocytosis, clathrin mediated endcocytosis and macropinocytosis respectively. N2A cells were seeded at a density as mentioned above. After 24 h, cells were preincubated with inhibitors at concentrations that were non-toxic to the cells. Caveolae mediated endocytosis was inhibited using nystatin at concentrations 20 μg/mL and 50 μg/mL. Chlorpromazine was used to inhibit clathrin-coated endocytosis at concentrations 1 μM and 5 μM. To inhibit macropinocytosis, colchichine was added at different concentrations (4 μM and 10 μM). Following the addition of inhibitors, FITC tagged TAT conjugated Rh-B-PNPs (RhBCp-PNP) were added at a concentration of 50 μg/mL. After 3 h incubation, media was removed, washed with PBS and visualized under the Leica microscope (Leica microsysytem, Germany).

Inhibition of macropinocytosis was further confirmed through FACS. For the flow cytometry experiment, cells were incubated with inhibitors for 24 h after reaching confluence. Media was then removed and fresh media containing blank NPs and NPCp along with colchichine was added and further incubated for three hours. Cells were then washed with ice cold PBS, trypsinized and used for the analysis (BD FACS Verse). NP and NPCp without inhibitor were treated as the internal controls.

2.14. *In vivo* study

BALB/c mice weighing 25 g were obtained from the institute as per IAEC (IAEC no. 06/2019 (B)). Mice were divided into three different groups: Saline control, Rh-B PNP and FITC-Cp Rh-B PNP. The animals were anesthetized with Isofluorine and the nanoparticles (20 mg/kg) were intravenously injected into the animals. The animals were imaged using the animal imaging system (Newton 7.0, Vilber) at different time points to understand the bioavailability of the nanoparticles. After 4 h, the animals were sacrificed and organs such as brain, liver and Kidney were surgically removed for further analysis. The tissues were fixed in a solution of 10% neutral buffered formalin followed by embedding in paraffin according to routine laboratory techniques. Sections of 5 μm thickness were diced and stained with Hematoxylin-Eosin (H&E). DAB HRP Brown detection system was used for immunohistochemical staining of AHNAK.

2.15. Statistics

All the experiments were repeated thrice and the results were expressed as mean with standard deviation. Student's t test (paired) was used to analyze significance using GraphPad. p value lesser than $p \leq 0.05$ was considered statistically significant.

3. Results and discussion

3.1. Optimization of nanoparticle synthesis parameters

Size of the nanoparticles plays a major role in their biodistribution, bioavailability, degradation, toxicity *etc*. In addition, size determines the rate of cellular uptake of the nanoparticles which is vital for the effective delivery across the blood-brain continuum. Hence, it is essential to synthesize the nanoparticles in an optimal size for the pre-transcytosis circulation of the nanoparticles.[23] PLGA Nanoparticles were synthesized using two methods: solvent emulsion and nano-precipitation method. Since nano-precipitation yielded nanoparticles of good size and stability, it was further standardized and used (Figure 1). Size of the PLGA NPs is influenced by polymer concentration, co-polymer ratio, solvent nature and surfactant. Previous results show that the co-polymeric ratio did not have huge impact on the size of the nanoparticles but increasing the polymeric concentration from 0.1%-10% yielded particles with increasing mean size.[23,24] Concomitantly, we have observed that decreasing the polymeric concentration from 2.5% to 0.25% yielded nanoparticles of good size and stability (data not shown). Besides, the solvent combination played a significant role in determining the size of the nanoparticles. Acetone alone yielded nanoparticles of larger size. Many reports suggest combinatorial solvent with acetone as a major component for synthesizing PLGA nanoparticles.[25] We have observed that DCM:Acetone:Methanol mix yielded good quality nanoparticles without much loss during nanoprecipitation and lyophilization. Moreover, increasing the acetone concentration in this solvent combination reduced the nanoparticle size by about two folds (Table No 1). Hence, we have standardized the solvent combination DCM:Acetone:Methanol at the ratio of 0.5:20:5 and used for further experiments.

3.2. Characterization of the synthesized nanoparticles

Nanoprecipitation yielded particles of the size 70 ± 10 nm with narrow particle size distribution. For the Rhodamine encapsulated nanoparticles the size was around 150 ± 10 nm implicating the increase in size was due to loading of Rhodamine B in the nanoparticles (Figure 1(b)). It has been reported that nanoparticles within the range of 70-200 nm are optimal for *in vivo* applications and the nanoparticles obtained here can be effectively used as drug carriers.[23] Fluorescent microscopy also confirmed the loading of Rh-B in PLGA NPs (Figure 1(c)). The surface charge was around -21 mV and -13.8 mV for PLGA NP and Rh-B NP respectively, indicating good stability. The negative charge on the surface is attributed to the presence of carbonyl groups on the surface of the nanoparticles (Tables 1 and 2). Positive charge causes

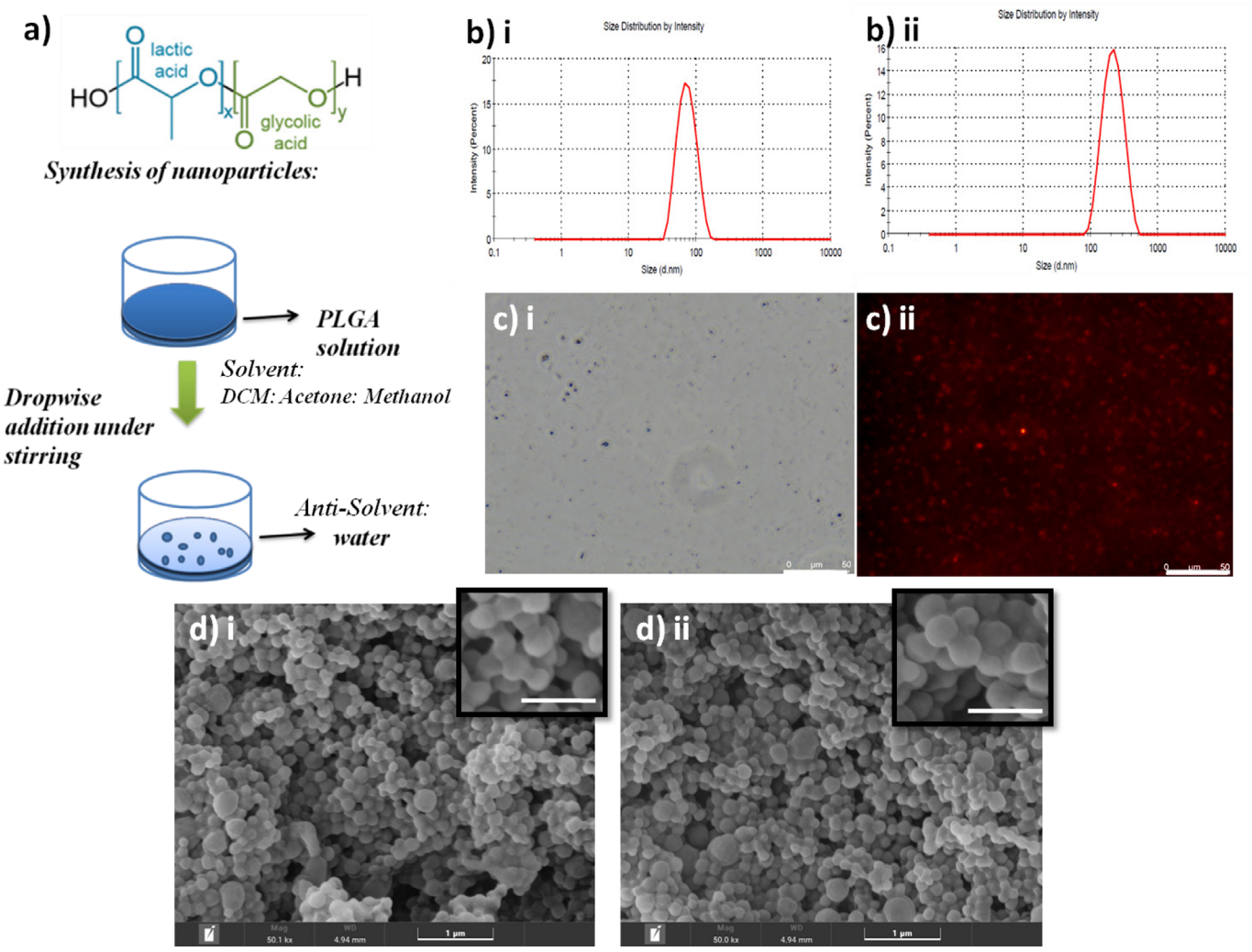

Figure 1. (a) Schematic representation of the synthesis of nanoparticles through nanoprecipitation. PLGA was dissolved in DCM:acetone:methanol (0.5:20:5) mixture and added dropwise into anti-solvent (water) at a solvent: antisolvent ratio of 1:2, (b) size of the nanoparticles as determined by zetasizer. (i) Size of PNP and (ii) Rh-B PNP. (c) Fluoresecent micrographs of rhodamine loaded PLGA nanoparticles (Rh-B PNP). Scale bar indicates 50 μm. (i) Phase contrast image and (ii) fluorescent image, (d) SEM image of (i) PNPs and (ii) Rh-B PNP. Scale bar indicates 1 μm. Insert shows the magnified images of the same. Scale bar of insert 500 nm.

Table 1. Optimization of the synthesis parameters of PLGA nanoparticles

Method	Solvent composition	Particle size (nm)	Zeta potential (mV)	PDI
Influence of preparation technique:				
Emulsion	DCM	548.6 ± 34	-33.5 ± 12	0.345
Nanoprecipitation	Acetone	345.3 ± 8	-10.6 ± 5.24	0.080
Influence of acetone concentration:				
Nanoprecipitation	DCM:Acetone:Methanol (0.5:5:5)	219.7 ± 15	-5.19 ± 4.6	0.158
Nanoprecipitation	DCM:Acetone:Methanol (0.5:5:10)	227 ± 10	-13.5 ± 0.5	0.012
Nanoprecipitation	DCM:Acetone:Methanol (0.5:15:5)	159.3 ± 2	-32.0 ± 11.6	0.002
Nanoprecipitation	DCM:Acetone:Methanol (0.5:20:5)	81.10 ± 6	-33.5 ± 12.4	0.196

Table 2. Optimizated parameters of PLGA nanoparticles, rhodamine-B loaded PLGA nanoparticles and TAT conjugated Rh-B PLGA nanoparticles

Sample name	Particle size (nm)	Zeta potential (mV)	PDI
PLGA nanoparticles (PNP)	69.19 ± 9	-21.6 ± 9.2	0.091
PLGA nanoparticles with rhodamine-B (Rh-B PNP)	169 ± 9	-13.5 ± 5.8	0.095
TAT conjugated rhodamine-B loaded PLGA nanoparticles (Rh-B CpPNP)	174 ± 8	-24.5 ± 11.7	0.814

immediate toxicity to the BBB and hence the presence of negative charge in the synthesized PLGA nanoparticle promotes enhanced passage of NPs across the BBB.[26] Further, the yield of the nanoparticle was found to be around 60%. Scanning electron microscopy also confirmed the size of the nanoparticles and the surface morphology was observed to be spherical (Figure 1(d)).

3.3. Conjugation of cell penetrating peptides to the nanoparticles and characterization

To increase the uptake of nanoparticles across the blood-brain barrier, cell penetrating peptides are being conjugated to the nanoparticles.[27,28] Cell penetrating peptides (Cpp) are cationic peptides that can be conjugated for the targeted delivery of cargos. Various cell penetrating peptides have been linked to the nanoparticles after the discovery of the TAT peptide from the HIV virus. However, TAT peptide sequence from 46-57 has been used extensively for delivering drugs to the blood-brain barrier. This region of TAT peptide is rich in arginine and lysine rendering it positively charged and hence assist in effective uptake by the cells.[29,30] TAT-peptide conjugated delivery of anti-HIV drugs demonstrated that even larger molecules can be transported across the BBB.[14] Hence, TAT peptide was used for efficient delivery of the nanoparticles across the BBB.

Peptide conjugation was confirmed through XPS analysis. The binding energy peaks at 279-298 eV, 392-410 eV, and 525-538 eV in XPS were ascribed to the elements C1s, N1s, and O1s, respectively. The binding energies of the respected elements are given in Table 3. It is evident from Figure 2(a)-(ii), that the N1 peak was not observed in the control nanoparticles. Thus the peak that corresponds to the N1 in Figure 2(a)-(iii), clearly represents the conjugation of peptide to the nanoparticle. To further understand the conjugation, TAT peptide with FITC labeling was conjugated to the PLGA NPs as described in the previous section. Fluorescent micrographs show that TAT peptide is being effectively conjugated to the nanoparticles (data not shown). Dynamic light scattering data revealed that the conjugation of TAT peptide increased the hydrodynamic size of the nanoparticle (Rh-B Cp PNP). Moreover, peptide conjugation increased the stability of the nanoparticles as evident by the increase in zeta potential (Table 2). SEM results indicate that TAT peptide conjugation did not alter the morphology of the synthesized PNPs and Rh-B PNPs (Figure 2(b)-(i)-(ii)).

FTIR analysis revealed the groups present in the nanoparticles. The broad peak around 3430 cm^{-1} confirms the presence of -OH group in PLGA (Figure 2(c)).[31] The sharp peak around 1745 cm^{-1} indicated the fingerprint stretching of the C=O ester carbonyl group in the PLGA copolymer and is a characteristic peak for PLGA polymer.[32,33] The peaks 2995 and 2945 cm^{-1} indicate symmetric and asymmetric stretching of C-H bond respectively. RhB spectrum showed weak peaks around 2990-2850 cm^{-1} indicates stretching vibrations of aromatic C-H.[34] Bands around 1687 cm^{-1} and 1636 cm^{-1} indicate C=O and C=C stretching respectively. Further, from Figure 2(c), we could observe benzene ring vibrational peaks around 1587-1463 cm^{-1}.[35,36] Rh-B PNP showed characteristic peaks for both PLGA (1745 cm^{-1}) and triple peaks of Rh-B (2990-2850 cm^{-1}) that indicates the loading of the dye in the nanoparticle. TAT conjugated Rh-B PNP also showed the triple peak indicating Rh-B incorporation (Figure 2(c)). Conjugation of TAT peptide to the nanoparticle was evident from the shift in the C=O peak (1752 cm^{-1}). Hence, FTIR data revealed the characteristic peaks for Rh-B incorporation and TAT peptide conjugation to the PLGA nanoparticle.

Quantitative assessment of the peptide conjugation with the nanoparticle is an important aspect to determine the bioavailabilty of nanoparticles across the BBB. Hence, TNBS (2,4,6-trinitrobenzene sulfonic acid) assay was used to understand the degree of peptide functionalization to the nanoparticles. TNBS reacts to the free amino groups generating a chromogenic product that can be measured at 335 nm.[37] Peptide tagged nanoparticle showed 25% percentage decrease in the free amine groups compared to the control (data not shown). Thus TNBS assay assorted the conjugated nanoparticles from the unconjugated peptides thereby presenting a quantitative data about the percentage of peptide conjugation to the nanoparticle.

3.4. Release behavior and biostability of rhodamine B loaded PLGA nanoparticle

The loading efficiency of Rh-B into the nanoparticle was determined using fluorescent spectroscopy. The loading of the Rhodamine-B in PLGA NPs was observed to be around 40%. The release kinetics was measured for a period of 24 h and from Figure 3(a), it is clear that merely 30% of the rhodamine has been released after 4 h and hence this dye can be used as a marker to track the bioavailability of nanoparticles inside the cell. This is in accordance with previous studies wherein slow release of dyes from the PLGA nanoparticles were reported.[38] However, after the 10^{th} hour, there is a gradual increase in the release pattern suggesting the ability of the nanoparticle to release the drug in a time controlled manner. It should also be noted that almost 70% of the dye has been released from the nanoparticle by 24^{th} hour ensuring the efficacy of this nanoparticle for short term delivery of drugs for neurodegenerative disorders.

Table 3. Binding energy peak values of oxygen (O1s), carbon (C1s), and nitrogen (N1s) in PNP and Cp PNP nanoparticles

		PNP			Cp PNP		
S. No	Binding Energy (BE)	O1s	C1s	N1s	O1s	C1s	N1s
1.	Start (eV)	537.86	298	0	538.84	298	410
2.	Peak (eV)	532.04	284.88	0	532.25	285.55	398.82
3.	End (eV)	526.26	279	0	525.84	279	392
4.	Height of peak	482133.67	279736.01	0	739772.84	318886.04	3759.33

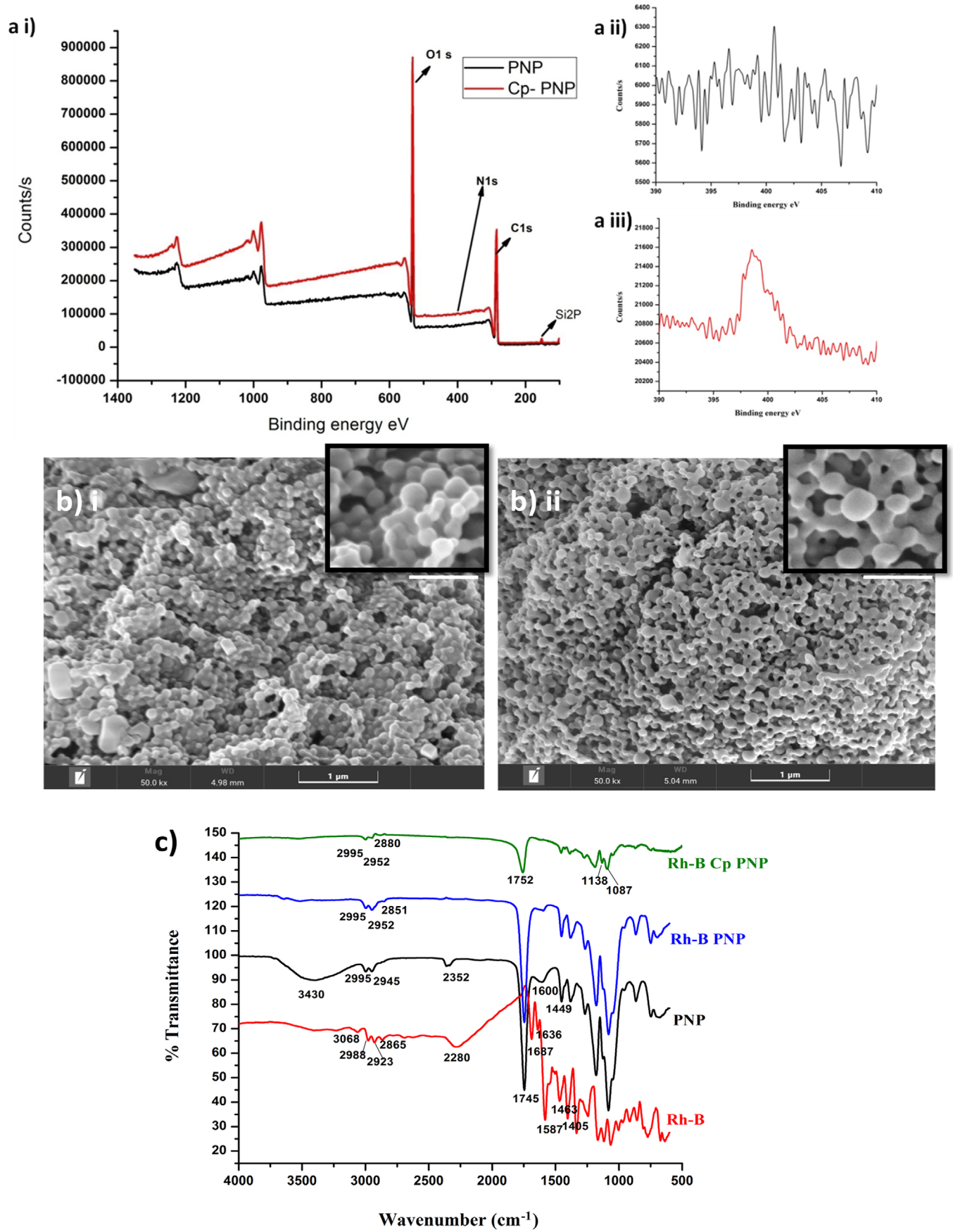

Figure 2. (a) XPS analysis of the synthesized nanoparticles: (a-i) Total XPS spectrum of the nanoparticles. Black represents PLGA NPs and red line represents TAT conjugated PLGA NPs (Cp PNP), (a-ii) nitrogen spectrum of PLGA NP, (a-iii) nitrogen spectrum of Cp-PNP, (b) SEM images of TAT peptide conjugated nanoparticles. (i) Rh-B PNPs, (ii) Rh-BCp PNP. Scale bar indicates 1 µm. Insert shows the magnified images of the same. Insert scale bar 500 nm, (c) FT-IR spectra of PNP, Rh-B PNP, and Cp-PNP.

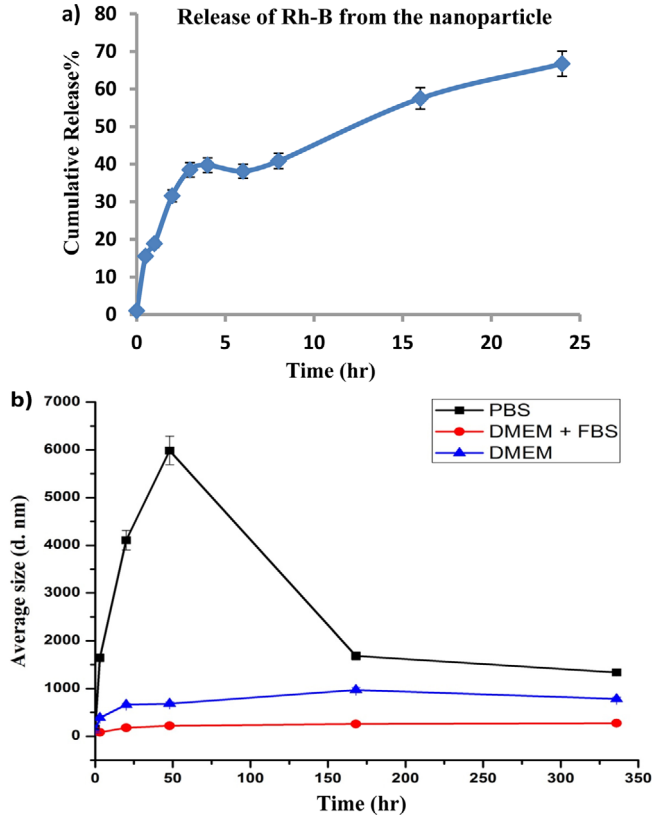

Figure 3. (a) Release profile of Rh-B from PLGA nanoparticles at different time intervals. (b) Biostability of the synthesized PLGA NPs (CpRh-B PNP) in PBS, DMEM and DMEM with FBS. Black line represents stability in PBS, blue line represents stability in DMEM and red line indicates nanoparticle stability in DMEM with FBS.

Nanoparticles tend to aggregate in biological systems and aggregated particles can block the blood vessels.[39] Hence, the size distribution of the TAT conjugated nanoparticles (RhBCp-PNP) were checked to understand the stability of nanoparticles in PBS (pH 7.4), DMEM and DMEM with 10% FBS. The nanoparticles aggregated within 24 h in PBS. Moreover, nanoparticles start to disintegrate within a week in PBS buffer (Figure 3(b)). Serum free media (DMEM) and DMEM supplemented with serum showed uniform stability for the period investigated (2 weeks). Besides, it is evident from figure 3b, that DMEM supplemented with serum (DMEM with FBS) showed lesser scattering indicating better stability than the DMEM and PBS.[39-44] Thus this result proves that the nanoparticles are stable in DMEM with FBS and hence can be used for biological evaluation.

3.5. Biocompatibility of the nanoparticles

The synthesized nanoparticles were checked for biocompatibility using the MTT assay. Neural precursor cells (N2A) were used to understand the effect of nanoparticles on neural cell toxicity. At 10 μg/mL and 50 μg/mL concentrations, nanoparticles seemed to promote proliferation of the cells and at 100 μg/mL there was around 80% viability. As evident from Figure 4(a), the Rh-B loaded nanoparticles and the peptide conjugation did not exert any toxic activity till 100 μg/mL concentration. Systemic delivery of the drugs or nanocarriers require blood compatibility. Hence, the bio-compatibility of the nanoparticles with the red blood cells through hemolysis assay was assessed. It is evident from the Figure 4(b), that the nanoparticles did not lyse the red blood cells and the percentage of hemolysis was within the permissible limit (5%) proving that this nanoparticle based drug carrier can be used in an *in vivo* system.[45] These results make PLGA NPs an excellent candidate for drug delivery.

Acridine orange can penetrate metabolically active cells, thereby staining the nucleic acid green while Propidium Iodide (PI) stains the non-viable cells red since PI cannot penetrate metabolically active cell. Therefore to understand whether the peptide conjugated nanoparticles had any effect on the membrane integrity, Acridine orange and Propidium Iodide staining were used. From Figure 4(c), it is clear that the permeability of PI was restricted in metabolically active cells treated with TAT-conjugated NPs. Moreover, the effect of concentration of the TAT-conjugated nanoparticles (Cp-PNP) on cell compatibility was checked with increasing the concentration of the peptide tagged nanoparticle. It has been evident from Figure 4(d), that increasing the nanoparticle concentration did not exert any toxicity. The dose dependent study of the nanoparticle compatibility is crucial for designing an effective drug delivery carrier. Thus this confirms that the peptide decorated nanoparticles are suitable delivery carriers to the brain.

3.6. *In vitro* uptake of nanoparticles

Size, composition, surface charge *etc.* of the nanoparticles play a crucial role in the cellular uptake.[31,46] Behzadi *et al.* show that the nanoclusters have more potential to be engulfed inside the cell rather than single nanoparticles. Besides, effect of surface modifications also play a crucial role in the internalization of the nanoparticles. Hence, the cellular uptake of the nanoparticles were determined through Flow cytometry analysis and Fluorescent imaging.

The flow cytometry data revealed that there was more than 30% increase in the uptake of TAT conjugated nanoparticles by the cells compared to the control nanoparticles (Figure 5(a),(b)). This indicates that the surface modifications enabled better uptake of nanoparticles by the cells. It is also clear from the flow cytometry data that the increased size of nanoparticles because of the loading of Rhodamine had no significant effect on the nanoparticle uptake after the peptide conjugation (Figure 5). Further to understand the uptake of the TAT conjugated nanoparticles, neuroblastoma cells were incubated with FITC-Cp Conjugated Rh-B PLGA (FITC-Cp Rh-B PNP) nanoparticles. From the fluorescent micrographs, it is clear that the TAT conjugated rhodamine loaded nanoparticles were promptly taken up by the cells (Figure 6(a)). These data prove that TAT peptide enhances the cellular level uptake of nanoparticles with the dye.

TAT particularly localizes proteins to the nuclei by acting as nuclear localization signals (NLS) and reports suggest that NPs tagged with TAT are localized to the nuclei.[15] However, in our experiment we could not observe nuclear localization of either the TAT-FITC peptide (Figure 6(b), (i-iii)) or the TAT-FITC conjugated Rhodamine loaded PNP (Figure 6(b), (iv-vi)). The fluo-

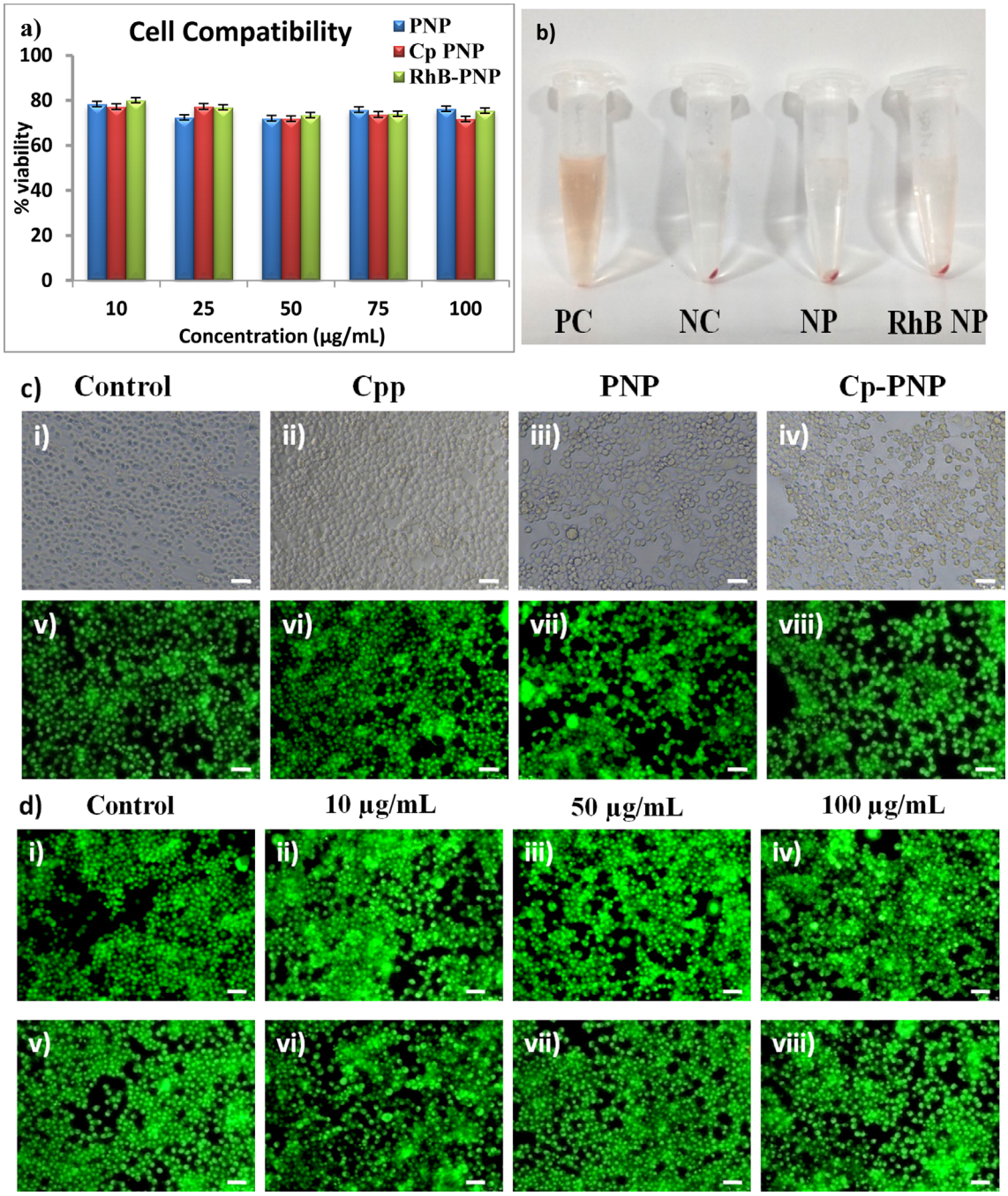

Figure 4. Biocompatibility of PLGA nanoparticles. (a) MTT assay, (b) hemocompatibility assay, (c) AO/PI analysis of TAT peptide (ii,vi), PNPs (iii, vii), PNPs conjugated with TAT peptide (iv,viii), (d) AO/PI assay with increasing concentration of PNPs. i-iv represents PLGA NP at varying concentration, v-viii represents PLGA NPs conjugated with TAT peptide at varying concentrations. Scale bar represents 50 µm.

rescent micrographs indicate that the nanoparticles were clearly localized in the cytoplasm (white arrows). This result is particularly important owing to the fact that nuclear localization might affect the differential gene expression. However, for the treatment of diseases that require modulation of the gene expression using drugs, further experiments should be conducted. Moreover, the relative intensity of the FITC-TAT conjugated to the nanoparticle (FITC-CpRhB PNP) was around 10% higher compared to the FITC-TAT (FITC-Cp) peptide itself indicating that the nanoparticles tagged to the peptide are readily taken up by the cells, corroborating the results by Behzadi *et al.* (Figure 6(c)). Thus this data reveals the significance of using TAT peptide conjugated PLGA nanoparticle for the delivery of therapeutic moieties.

3.7. Inhibition of uptake of nanoparticles by the cells

Cpp conjugated nanoparticle uptake by the cells have been initially considered to be a passive direct penetration. However, after 2003 many groups proposed endocytic internalization of cpp conjugated NPs.[28] Cellular uptake is primarily driven by endocytosis which further can be grouped into two distinct mechanisms: pinocytosis and phagocytosis. Phagocytosis is the

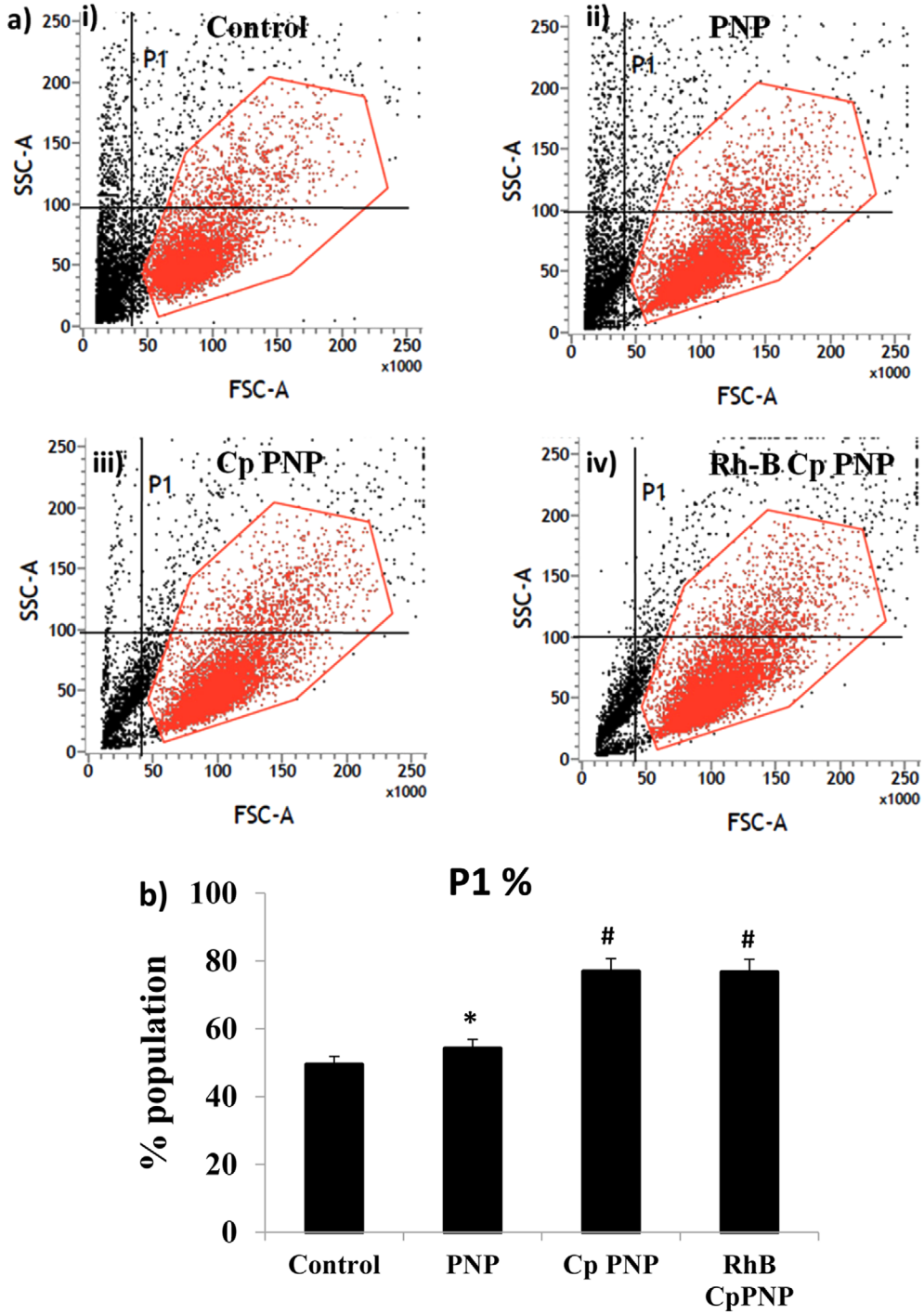

Figure 5. Uptake of the synthesized nanoparticles by flow cytometry. (a) Flow cytometry data of Control cells (i), PNPs (ii), Cp PNP (iii), Rh-B Cp PNP (iv). (b) Percentage of cells that has taken up the nanoparticles. $p \leq 0.05$ is denoted by * and $p \leq 0.01$ denoted by # when compared with control.

principal route of uptake by immune cells like macrophages, neutrophils and monocytes. Pinocytosis include different pathways like clathrin coated endocytosis, caveolae mediated endocytosis, macropinocytosis and clathrin/caveolae independent endocytosis. TAT uptake by the cell is proposed to be of micropinocytosis.[28,29,44,47] Hence, to understand the uptake route inside the cell, inhibitors for each of the pinocytosis pathways were used. Caveolae mediated endocytosis is inhibited by the drug nystatin (NY) which disrupts the lipid rafts.[48,49] Chlorpromazine (CPZ) is a cationic drug and has been widely used to inhibit clathrin coated endocytosis because of its ability to relocate clathrinand adaptor protein 2 (AP2) from plasma membrane to endosomes.[16,44,49,50] Colchichine (Col) is a macropinocyte inhibitor by exerting its effect on the microtubule polymerization thereby affecting the endocytosis.[16,51,52] Inhibitors for each of the pathway was used in different concentrations and the cellular internalization was understood through fluorescent microscopy. Fluorescent micrographs reveal that the uptake of nanoparticles

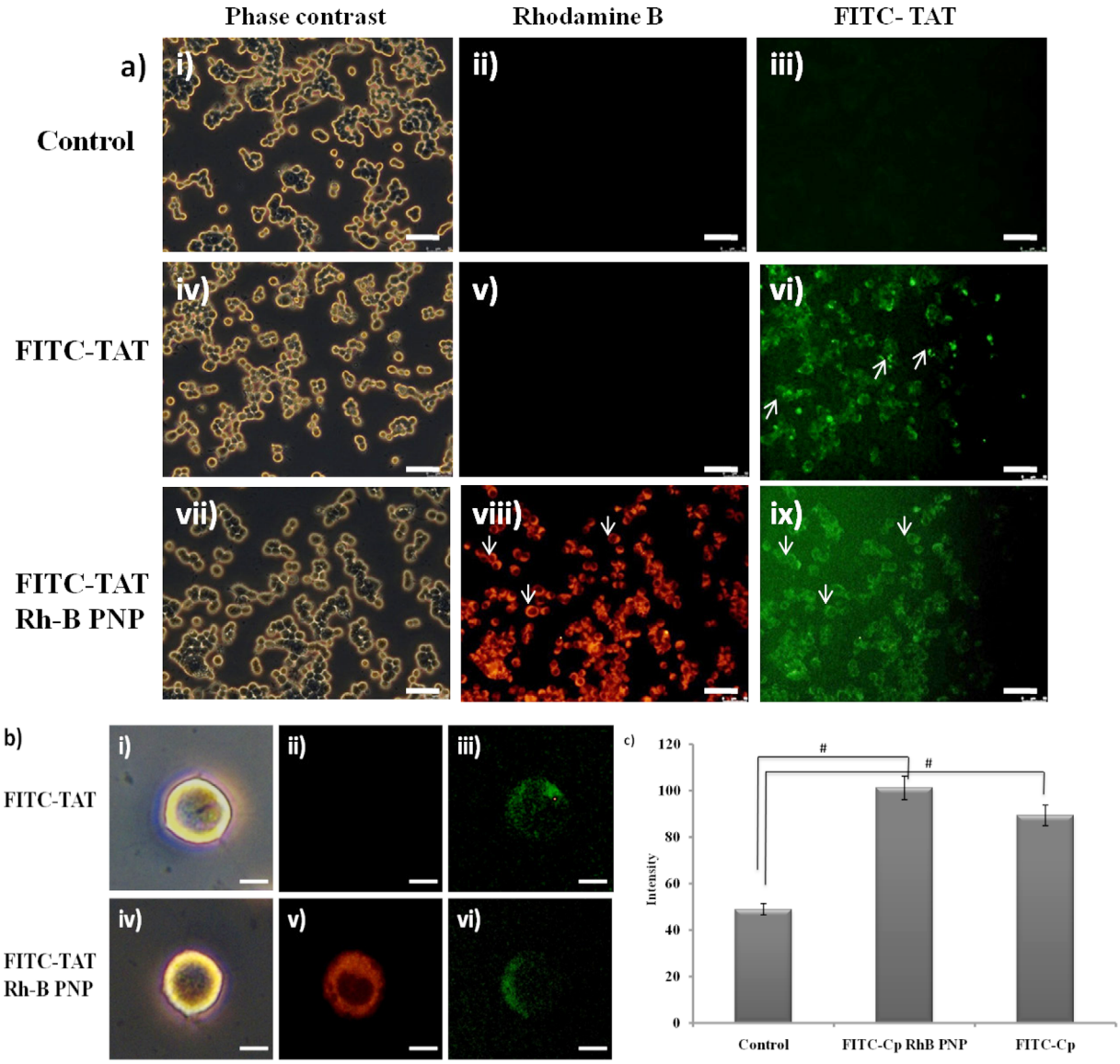

Figure 6. (a) Fluorescent images of nanoparticle uptake. Control cells (i-iii), FITC-TAT peptides (iv-vi), Rh-B loaded FITC-TAT conjugated nanoparticles (vii-ix). Scale bar represents 50 μm. (b) Single cell image of cellular uptake of nanoparticles. (i-iii) FITC-TAT peptides alone (FITC-Cp), (iv-vi) Rh-B loaded FITC-TAT conjugated nanoparticles (FITC-Cp Rh-B PNP). Scale bar represents 25 μm. (c) Relative intensity of the FITC-TAT peptide and Rhodamine loaded FITC-TAT conjugated nanoparticles. p value $\leq$ 0.001 represented by #.

was not affected when the cells were treated with NY or CPZ (Figure 7(a)). Besides, it was also observed that further increasing the concentration of the inhibitors had an effect on the viability of the cells. However, from Figure 7(a), it is clear that Col treatment inhibited the internalization of nanoparticles inside the cell in a concentration dependent manner. Thus this data proves that TAT-conjugated NPs (Rh-B Cp PNP) are internalized through macropinocytosis.

To further confirm the mechanism of uptake of NPs, inhibition of macropinocytosis pathway by specific inhibitor was performed. Since TAT mediated endocytosis is primarily through macropinocytosis, the percentage of inhibition of micropinocytosis by colchicine on nanoparticle uptake was studied through flow cytometry. Figure 7(b) reveals that colchicine treatment reduced the uptake of nanoparticles proving that indeed TAT peptide mediated uptake happens through macropinocytosis. Furthermore, increasing the concentration of colchichine (10 μM) had a negative influence on the viability and the uptake of the nanoparticles (Figure 7(b)).

3.8. *In vivo* analysis of the synthesized nanoparticles

Polymers or nanoparticles crossing the BBB were mostly understood through the residual drugs that are present in the *ex-vivo* brain section of animals.[4,8,10,14,53] *In vivo* fluorescent imaging of brain is challenging because of the difficulty of the imaging systems in penetrating the skull region and the relatively lesser fluorescence that emanates from the fluorescent moieties. Moreover, imaging requires the animals in a fixed live condition to understand the kinetics. Hence we have standardized the fluorophore, the efficient concentration for effective imaging and the time point where optimal fluorescence was obtained.

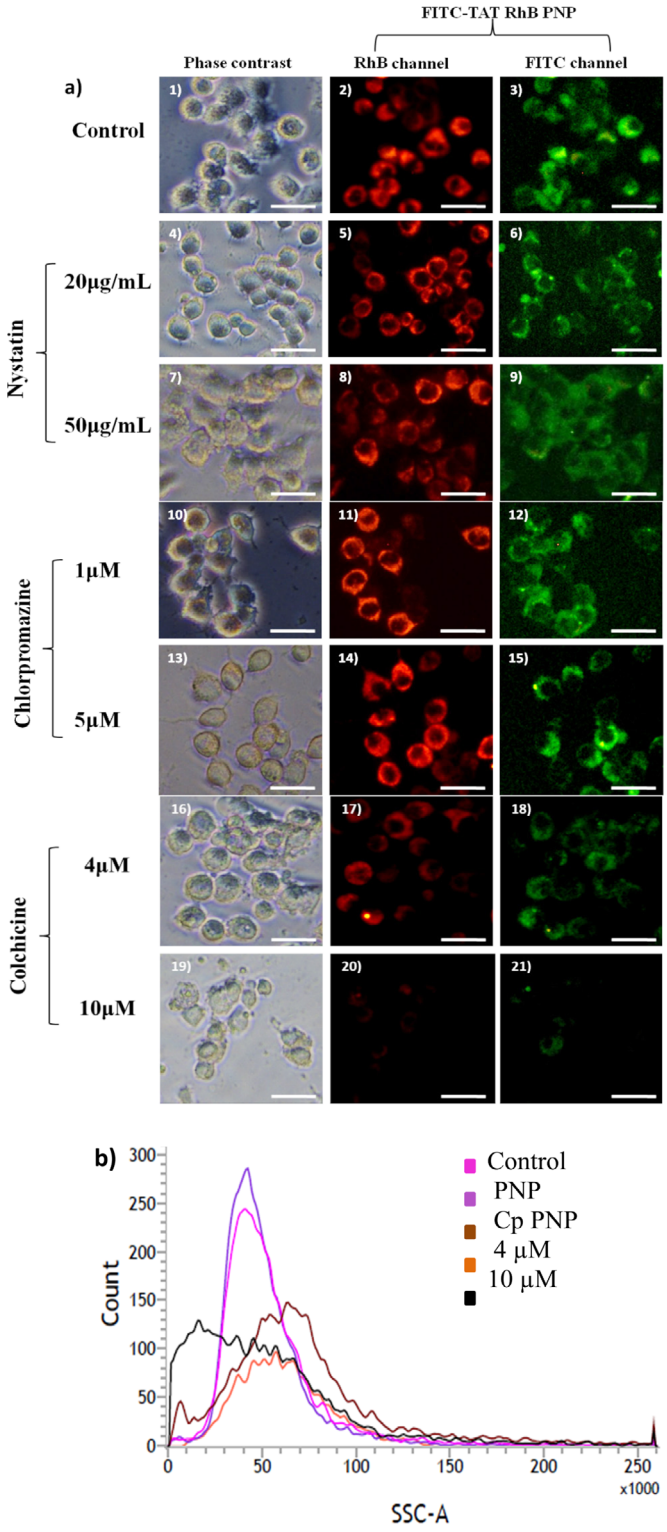

Figure 7. Uptake inhibition of the peptide tagged nanoparticles. (a) Fluorescent micrographs of uptake inhibition with increasing concentration of inhibitors for caveolae mediated uptake (nystatin-20 μg/mL (4-6) and 50 μg/mL (6-8)), clathrin mediated endocytosis (chlorpromazine-1 μM (9-11) and 5 μM (12-14)) and macropinocytosis uptake (colchicine-4 μM (15-17) and 10 μM (18-20)). Red channel represents Rhodamine in the RhBCp-PNPs and green channel represents FITC-TAT in the RhBCp PNPs. Scale bar represents 100 μm, (b) Flow cytometry data for macropinocytosis inhibition by colchicineat increasing concentration (4 μM and 10 μM).

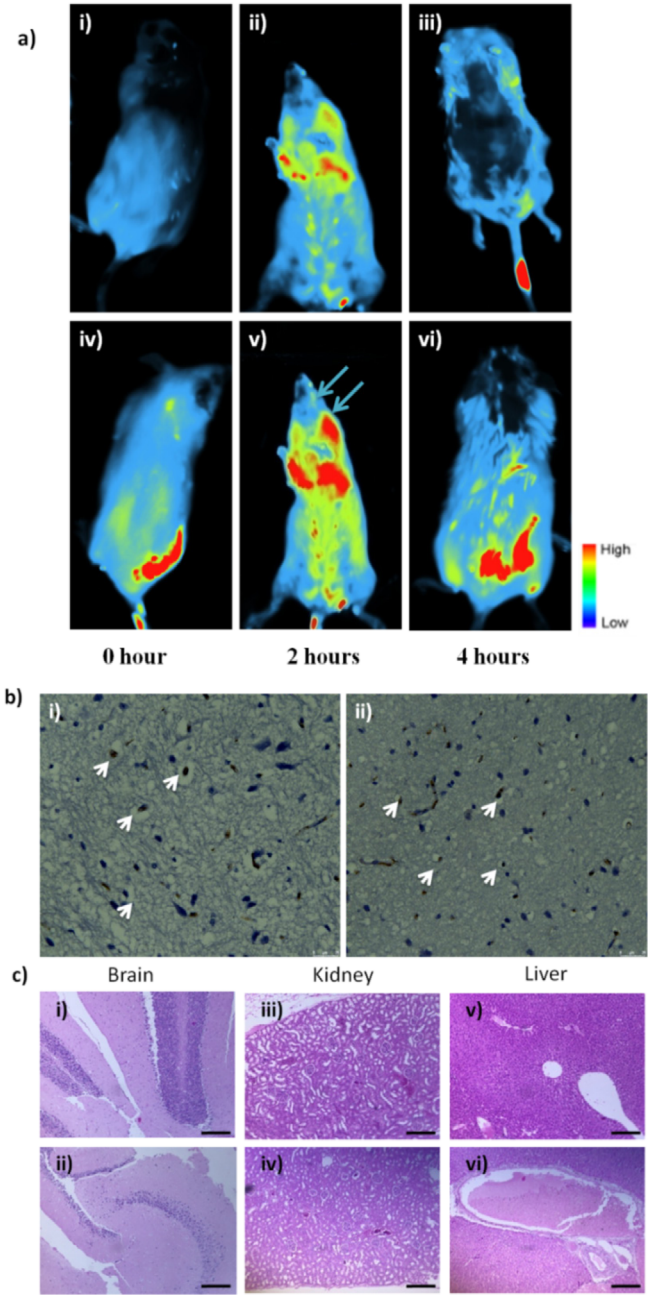

Figure 8. *In vivo* analysis of the peptide-tagged nanoparticles. (a) *In vivo* imaging of the PLGA NPs (i-iii), TAT conjugated PLGA NPs (iv-vi). (i) & (iv) represents the images taken at 0 hour, (ii) & (v) represents the images taken after 2 hours and (iii) & (vi) represents the images taken after 4 hours of injection. (b) Immunostaining of the *ex-vivo* brain section with AHNAK antibody. (i) Saline control (ii) TAT-conjugated PNPs. Scale bar represents 50 μm, (c) H & E staining of various organs like Brain (i,ii), Kidney (iii,iv) and Liver (v,vi) isolated from Saline control mice (i,iii,v), TAT-conjugated PNPs (ii,iv,vi). Scale bar represents 250 μm.

Animals were divided into three groups: saline control, rhodamine loaded nanoparticles, FITC-Cp conjugated nanoparticles. The control animals only received saline and was used as a control to reduce background fluorescence. The rhodamine loaded nanoparticles could not be visualized using the animal imaging system and hence we have used FITC along with rhodamine in the nanoparticle for the imaging. It is clear from the *in vivo* imag-

ing that the peptide conjugated nanoparticles have reached the brain by two hours (Figure 8(a), (v) indicated by arrows). Besides, it is clear from the figure that by 4 h, renal clearance of the nanoparticles were observed (Figure 8(iii), (vi)). Hence, this study advocates faster delivery of the drugs to the BBB and quicker clearance thus proving to be a prudent carrier for the treatment of neurodegenerative disorders.

To further understand the integrity of the blood-brain barrier after the nanoparticle entry, we have stained the brain sections with the BBB marker AHNAK. AHNAK is co-localized with the Zona-occludens (ZO-1) in the capillary of brain cells compared to the endothelium of capillaries where there is active exchange between the blood and cells. This exemplifies AHNAK as a marker for endothelium with barrier properties.[54] The immunohistochemical data staining with AHNAK revealed that the nanoparticle entry did not affect the barrier properties (Figure 8(b)).

Several reports show that the cell penetrating peptide modulates the inflammatory pathway thereby leading to apoptosis.[47] Therefore we have isolated the organs, specifically brain, liver and the kidney to understand the inflammatory responses. Histo-chemical analysis showed that the nanoparticles did not exert any toxicity to the brain (Figure 8(c)). There was no necrosis or inflammtion in the liver and kidney, suggesting that the synthesized nanoparticle is biocompatible in an *in vivo* model and can be further used as a drug delivery carrier for transporting drugs across the blood-brain barrier.

The *in vitro* cell uptake studies and the NP bioavailabilty in the mice model corroborate the potential of the synthesized nanoparticle to be used as an effective drug delivery vehicle for efficient traversing of the BBB. However, future experiments will determine the efficacy and the *in vivo* bioavailability of the drugs to be administered for various disorders.

4. Conclusions

Development of new approach for treating neuro-degenerative disorders is an intricate, expensive and challenging niche. However, very few therapeutics for brain-targeted delivery have reached clinical trials. In this report, we have synthesized rhodamine loaded PLGA nanoparticles through solvent displacement method and these nanocarriers were of smaller in size, biocompatible and offers sustained drug release. Cell penetrating peptide TAT was used to enhance the delivery to the BBB and our *in vitro* data supports the enhanced uptake of peptide conjugated nanoparticles. In recent years, numerous *in vitro* model for the BBB have been developed to replicate the barrier. However, *in vivo* models are required to provide insights into the complexity of the BBB and clinical relevance. Further, only metallic nanoparticles have been used to track nanoparticle bioavailabilty in *in vivo* systems through imaging. Nevertheless, inorganic NPs have some disadvantages such as NP accumulation, degradation and undesired toxicity at higher concentrations. Albeit tracking polymeric nanoparticle uptake in an *in vivo* model has numerous challenges, we have successfully synthesized a nanocarrier system for imaging NP bioavailabilty in a mice model. Moreover, the nanoparticles were administered to the brain without any accumulation or disruption of the blood-brain barrier. In conclusion, we have demonstrated the size and conjugation of peptides have remarkable impact on the cellular uptake and specific distribution compared to the unconjugated nanoparticles in an *in vivo* system through fluorescent live animal imaging.

Conflict of interest: The authors declare no conflict of interest.

References

(1) J. Li and C. Sabliov, *Nanotechnol. Rev.*, **2**, 241 (2013).
(2) L. Chen, D. Zeng, N. Xu, C. Li, W. Zhang, X. Zhu, Y. Gao, P. R. Chen, and J. Lin, *ACS Appl. Mater. Interfaces*, **11**, 41889 (2019).
(3) H. Song, M. Wei, N. Zhang, H. Li, X. C. Tan, Y. J. Zhang, and W. S. Zheng, *Int. J. Nanomedicine*, **13**, 1869 (2018).
(4) J. Li, L. Feng, L. Fan, Y. Zha, L. Guo, Q. Zhang, J. Chen, Z. Pang, Y. Wang, X. Jiang, V. C.Yang, and L. Wen, *Biomaterials*, **32**, 4943 (2011).
(5) S. Fan, Y. Zheng, X. Liu, W. Fang, X. Chen, W. Liao, X. Jing, M. Lei, E. Tao, Q. Ma, X. Zhang, R. Guo, and J. Liu, *Drug Deliv.*, **25**, 1091 (2018).
(6) M. Malhotra, C. Tomaro-duchesneau, and S. Prakash, *Biomaterials*, **34**, 1270 (2013).
(7) Y. Li, Y. Pei, X. Zhang, Z. Gu, Z. Zhou, W. Yuan, J. Zhou, J. Zhu, and X. Gao, *J. Control. Release*, **71**, 203 (2001).
(8) G. Tosi, L. Costantino, F. Rivasi, B. Ruozi, E. Leo, A. V. Vergoni, R. Tacchi, A. Bertolini, M. A. Vandelli, and F. Forni, *J. Control. Release*, **122**, 1 (2007).
(9) A. Jonderian and R. Maalouf, *Front. Pharmacol.*, **7**, 458 (2016).
(10) J. Kennedy, E. Larrañeta, M. T. C. Mccrudden, C. M. Mccrudden, A. J. Brady, S. J. Fallows, H. O. McCarthy, A. Kissenpfennig, and R. F. Donnelly, *J. Control. Release*, **265**, 57 (2017).
(11) M. Salvalaio, L. Rigon, D. Belletti, F. D'Avanzo, F. Pederzoli, B. Ruozi, O. Marin, M. A. Vandelli, F. Forni, M. Scarpa, R. Tomanin, and G. Tosi, *PLOS ONE*, **11**, e0156452 (2016).
(12) S. Maya, L. G. Kumar, B. Sarmento, N. S. Rejinold, D. Menon, S. V. Nair, and R. Jayakumar, *Carbohydr. Polym.*, **93**, 661 (2013).
(13) S. Neves-Coelho, R. P. Eleutério, F. J. Enguita, V. Neves, and M. A. R. B. Castanho, *Molecules*, **22**, 1753 (2017).
(14) K. S. Rao1, M. K. Reddy, J. L. Horning, and V. Labhasetwar, *Biomaterials*, **29**, 4429 (2008).
(15) Y. S. Nam, J. Y. Park, S.-H. Han, and I.-S. Chang, *Biotechnol. Lett.*, **24**, 2093 (2002).
(16) K. Hu, Y. Shi, W. Jiang, J. Han, S. Huang, and X. Jiang, *Int. J. Pharm.*, **415**, 273 (2011).
(17) S. K. Samal, M. Dash, P. Dubruel, K. Müllen, and J. Rajadas, in *Cationic Polymers in Regenerative Medicine*, S. Samal and P. Dubrue, Eds., The Royal Society of Chemistry, 2015, Chap. 20, pp 539-556.
(18) S. Behzadi, V. Serpooshan, W. Tao, M. A. Hamaly, M. Y. Alkawareek, E. C. Dreaden, D. Brown, A. M. Alkilany, O. C. Farokhzad, and M. Mahmoudi, *Chem. Soc. Rev.*, **46**, 4218 (2017).
(19) D. Y. Tam, J. W.-T. Ho, M. S. Chan, C. H. Lau, T. J. H. Chang, H. M. Leung, L. S. Liu, F. Wang, L. L. H. Chan, C. Tin, and P. K. Lo, *ACS Appl. Mater. Interfaces*, **12**, 28928 (2020).
(20) Y. Cheng, Q. Dai, R. A. Morshed, X. Fan, M. L. Wegscheid, D. A. Wainwright, Y. Han, L. Zhang, B. Auffinger, A. L. Tobias, E. Rincón, B. Thaci, A. U. Ahmed, P. C. Warnke, C. He, and M. S. Lesniak, *Small*, **10**, 5137 (2014).
(21) E. Barbu, E. Molnàr, J. Tsibouklis, and D. C. Górecki, *Expert Opin. Drug Deliv.*, **6**, 553 (2009).
(22) L. Liu, S. S. Venkatraman, Y.-Y. Yang, K. Guo, J. Lu, B. He, S. Moochhala, and L. Kan, *PeptideScience*, **90**, 617 (2008).
(23) Q. Cai, L. Wang, G. Deng, J. Liu, Q. Chen, and Z. Chen, *Am. J. Transl. Res.*, **8**, 749 (2016).

(24) C. E. Astete and C. M. Sabliov, *J. Biomater. Sci. Polym. Ed.*, **17**, 247 (2006).
(25) C. E. Astete and C. M. Sabliov, *J. Biomater. Sci., Polym. Ed.*, **17**, 247 (2006).
(26) C. Saraiva, C. Praça, R. Ferreira, T. Santos, L. Ferreira, and L. Bernardino, *J. Control. Release*, **235**, 34 (2016).
(27) I. Gessner and I. Neundorf, *Int. J. Mol. Sci.*, **21**, 2536 (2020).
(28) S. Silva, A. J. Almeida, and N. Vale, *Biomolecules*, **9**, 22 (2019).
(29) K. S. Rao, A. Ghorpade, and V. Labhasetwar, *Expert Opin. Drug Deliv.*, **6**, 771 (2009).
(30) S. W. Jones, R. Christison, K. Bundell, C. J. Voyce, S. M. V. Brockbank, P. Newham, and M. A. Lindsay, *Br. J. Pharmacol.*, **145**, 1093 (2005).
(31) S. Şimşek, H. Eroğlu, B. Kurum, and K. Ulubayram, *J. Microencapsul.*, **30**, 10 (2013).
(32) S. Streck, H. Neumann, H. M. Nielsen, T. Rades, and A. McDowell, *Int. J. Pharm. X*, **1**, 100030 (2019).
(33) J.-H. Park, J.-Y. Lee, U. Termsarasab, I.-S. Yoon, S.-H. Ko, J.-S. Shim, H.-J. Cho, and D.-D. Kim, *Int. J. Pharm.*, **473**, 426 (2014).
(34) U. Lamdab, K. Wetchakun, W. Kangwansupamonkon, and N. Wetchakun, *RSC Adv.*, **8**, 6709 (2018).
(35) W. Madami and R. Seoudi, *J. Taibah Univ. Sci.*, **14**, 790 (2020).
(36) L. Lu, X. Yue, F. Lin, F. Huang, B. Zhang, and Z. Lin, *J. Mater. Chem. A*, **3**, 10959 (2015).
(37) A. Satish and P. S. Korrapati, *J. Tissue Eng. Regen. Med.*, **13**, 753 (2013).
(38) T. Betancourt, K. Shah, and L. Brannon-Peppas, *J. Mater. Sci. Mater. Med.*, **20**, 387 (2009).
(39) D. T. Pham, N. Saelim, R. Cornu, A. Béduneau, and W. Tiyaboonchai, *Pharmaceuticals (Basel)*, **13**, 86 (2020).
(40) H. S. Han, T. Thambi, K. Y. Choi, S. Son, H. Ko, M. C. Lee, D.-G. Jo, Y. S. Chae, Y. M. Kang, J. Y. Lee, and J. H. Park, *Biomacromolecules*, **16**, 447 (2015).
(41) X. Liu, J. Cao, H. Li, J. Li, Q. Jin, K. Ren, and J. Ji, *ACS Nano*, **7**, 9384 (2013).
(42) Technology Cs, *TGF-β/Smad Signaling*, 2017.3; Available from: http://learn.cellsignal.com/hubfs/landing-pages/2016/2016-10_Cancer_Pathway_Handouts_new_version/Developmental_Biology/2016_04_TGF_PW_Handout-digital.pdf?hsCtaTracking=4d1ef20b-368e-4f3c-abe6-cfc4bfda2f38%7Cd8b2edd9-0a5a-4b60-9090-01bca188b8e5
(43) S. Jeon, H. Ko, N. V. Rao, H. Y. Yoon, D. G. You, H. S. Han, W. Um, G. Saravanakumar, and J. H. Park, *RSC Adv.*, **5**, 70352 (2015).
(44) J. Chang, Y. Jallouli, M. Kroubi, X.-B. Yuan, W. Feng, C.-S. Kang, P.-Y. Pu, and D. Betbeder, *Int. J. Pharm.*, **379**, 285 (2009).
(45) K. P. Sai, M. V. Jagannadham, M. Vairamani, N. P. Raju, A. S. Devi, R. Nagaraj, and N. Sitaram, *J. Biol. Chem.*, **276**, 2701 (2001).
(46) S. Salatin and A. Y. Khosroushahi, *J. Cell. Mol. Med.*, **21**, 1668 (2017).
(47) H. Kim, S. Moodley, and M. Liu, *Drug Deliv. Transl. Res.*, **5**, 275 (2015).
(48) S. Salatin and A. Y. Khosroushahi, *J. Cell Mol. Med.*, **21**, 1668 (2017).
(49) H. Tang, H. Chen, Y. Jia, X. Liu, Z. Han, A. Wang, Q. Liu, X. Li, and X. Feng, *Int. J. Nanomedicine*, **2017**, 6937 (2017).
(50) A. Sahin, G. Esendagli, F. Yerlikaya, S. Caban-Toktas, D. Yoyen-Ermis, U. Horzum, Y. Aktas, M. Khan, P. Couvreur, and Y. Capan, *Artif. Cells Nanomedicine Biotechnol.*, **245**, 1657 (2017).
(51) R. Mohammadpour, S. Safarian, B. Buckway, and H. Ghandehari, *Macromol. Biosci.*, **17**, 1600333 (2017).
(52) V. K. Yellepeddi, A. Kumar, and S. Palakurthi, *Anticancer Res.*, **29**, 2933 (2009).
(53) G. Joshi, A. Kumar, and K. Sawant, *Drug Deliv.*, **23**, 3492 (2016).
(54) B. J. Gentil, C. Benaud, C. Delphin, C. Remy, V. Berezowski, R. Cecchelli, O. Feraud, D. Vittet, and J. Baudier, *J. Cell. Physiol.*, **203**, 362 (2005).